Applied Catalysis B: Environmental 91 (2009) 516–523

Contents lists available at ScienceDirect

Applied Catalysis B: Environmental

journal homepage: www.elsevier.com/locate/apcatb

Ethanol oxidation reaction on $PtCeO_2/C$ electrocatalysts prepared by the polymeric precursor method

R.F.B. De Souza [a], A.E.A. Flausino [a], D.C. Rascio [a], R.T.S. Oliveira [a,b], E. Teixeira Neto [a], M.L. Calegaro [c], M.C. Santos [a,*]

[a] LEMN – Laboratório de Eletroquímica e Materiais Nanoestruturados – CCNH - Centro de Ciências Naturais e Humanas, UFABC - Universidade Federal do ABC, CEP 09.210-170, Rua Santa Adélia 166, Bairro Bangu, Santo André, SP, Brazil

[b] Faculdade de Ciências Exatas e Sociais Aplicadas, Campus II Universidade Federal dos Vales do Jequitinhonha e Mucuri - Rodovia MGT 367 – Km 583, n° 5000, Bairro Alto da Jacuba, 39100-000 Diamantina MG, Brazil

[c] Grupo de Materiais Eletroquímicos e Métodos Eletroanalíticos – Instituto de Química de São Carlos, Universidade de São Paulo, Caixa Postal 780, 13566-590 São Carlos, SP, Brazil

ARTICLE INFO

Article history:
Received 10 February 2009
Received in revised form 8 May 2009
Accepted 19 June 2009
Available online 26 June 2009

Keywords:
Ethanol oxidation reaction
Electrocatalysis
Pt nanoparticles
Ceria
Polymeric precursor method

ABSTRACT

This paper presents a study of the electrocatalysis of ethanol oxidation reactions in an acidic medium on Pt-CeO_2/C (20 wt.% of Pt-CeO_2 on carbon XC-72R), prepared in different mass ratios by the polymeric precursor method. The mass ratios between Pt and CeO_2 (3:1, 2:1, 1:1, 1:2, 1:3) were confirmed by Energy Dispersive X-ray Analysis (EDAX). X-ray diffraction (XRD) structural characterization data shows that the Pt-CeO_2/C catalysts are composed of nanosized polycrystalline non-alloyed deposits, from which reflections corresponding to the fcc (Pt) and fluorite (CeO_2) structures were clearly observed. The mean crystallite sizes calculated from XRD data revealed that, independent of the mass ratio, a value close to 3 nm was obtained for the CeO_2 particles. For Pt, the mean crystallite sizes were dependent on the ratio of this metal in the catalysts. Low platinum ratios resulted in small crystallites, and high Pt proportions resulted in larger crystallites. The size distributions of the catalysts particles, determined by XRD, were confirmed by Transmission Electron Microscope (TEM) imaging. Cyclic voltammetry and chronoamperometic experiments were used to evaluate the electrocatalytic performance of the different materials. In all cases, except Pt-CeO_2/C 1:1, the Pt-CeO_2/C catalysts exhibited improved performance when compared with Pt/C. The best result was obtained for the Pt-CeO_2/C 1:3 catalyst, which gave better results than the Pt-Ru/C (Etek) catalyst.

© 2009 Elsevier B.V. All rights reserved.

1. Introduction

Direct alcohol fuel cells (DAFC) have received much attention due to their potential applications in transportation and portable electronic devices [1–7]. DAFC use methanol or ethanol as fuel directly, without an external reformer, which makes them simple and compact [1]. Regarding DMFC (direct methanol fuel cells), there are two major obstacles that limit the practical application of these devices: (i) the relatively low dynamics of methanol electro-oxidation, and (ii) the high methanol crossover through the polymeric Nafion® membrane [8–10]. Similar problems are observed with DEFC (direct ethanol fuel cells), and in comparison with DMFC, are in an early stage of development. Despite these problems, DEFC have attracted much attention in recent years, mostly related to several advantages of using ethanol instead of methanol as fuel. Ethanol has a higher energy density than methanol (8.01 kWh kg^{-1} *vs.* 6.09 kWh kg^{-1}) [1,8]. Ethanol is also safer, can be easily produced in large quantities from biomass, and is considered a "green fuel". The development of new catalysts is particularly important for direct ethanol fuel cells (DEFCs), mainly due to their slow dynamics and poisoning of the catalyst surface by the several intermediates produced during the oxidation processes in both methanol and ethanol oxidation reactions [8,10,11]. From a practical viewpoint, the main obstacles for the development of DEFC are associated with several details closely related to the reaction mechanism. Research on new catalytic materials for DEFC requires a detailed knowledge of the reaction mechanism. Although the mechanism of ethanol oxidation is still unclear, or even contradictory in some points, it is well accepted that in acidic solutions the reaction proceeds through a series of parallel

* Corresponding author. Tel.: +55 11 4996 0163; fax: +55 11 4437 8530.
E-mail address: mauro.santos@ufabc.edu.br (M.C. Santos).

0926-3373/$ – see front matter © 2009 Elsevier B.V. All rights reserved.
doi:10.1016/j.apcatb.2009.06.022

reactions as summarized in the following scheme [12]:

$$CH_3CH_2OH \rightarrow [CH_3CH_2OH]_{ad} \rightarrow C1_{ad}, C2_{ad} \rightarrow CO_2 \text{ (total oxidation)} \quad (1)$$

$$CH_3CH_2OH \rightarrow [CH_3CH_2OH]_{ad} \rightarrow CH_3CHO \rightarrow CH_3COOH \text{ (partial oxidation)} \quad (2)$$

The complete electro-oxidation of ethanol to CO_2 involves the cleavage of the C–C bond. This requires rather high activation energy, and goes through two adsorbed intermediates, $C1_{ad}$ and $C2_{ad}$, which represent intermediates with one and two carbons, respectively.

Platinum-based materials are the most successful catalysts in DEFC anodes, especially PtRu, PtRuSn, and PtSn [13–17]. The combination of Pt with an oxophilic element is essential, since this allows for the activation of water at low potentials. This step provides oxygenated species that are necessary to oxidize some of the intermediates produced during the reaction, and avoids poisoning of the catalyst surface (the bi-functional mechanism). Several metal oxides, such as RuO_2 [18–20], WO_3 [21], ZrO_2 [22], MgO [23], and CeO_2 [24], have also been used to enhance the electrocatalytical activity toward ethanol or methanol electro-oxidation through a synergistic effect. Among these, rare earth oxides exhibit a number of characteristics that make them interesting in catalytic applications, such as ceria. Ceria has a fluorite oxide structure, where the metallic center surrounded by oxygen atoms is a cationic species capable of changing its oxidation state between +3 and +4. Ceria-based catalysts have been investigated for water–gas-shift reactions at low temperatures [25], and the good performance observed has motivated the use of such catalysts in fuel cell applications [8]. Several examples of the strong performance of ceria-based catalysts for methanol and ethanol oxidations in fuels cell systems have recently been reported in the literature [26–29]. The improved performance was attributed to a synergistic effect, and to the ability of ceria to supply sufficient OH_{ads} at low potentials, which is necessary to eliminate the poisoning species (especially CO_{ads}) formed during the methanol or ethanol oxidation reactions. It is important to point out that, to the best of our knowledge, only one paper [29] reports the ethanol oxidation in an acidic medium on Pt-CeO_2 electrodes. Although the catalytic performance of ceria-based catalysts for ethanol or methanol oxidation were similar to that obtained on PtRu catalysts, cerium oxide is an ideal substitute for ruthenium in such catalysts since it is much cheaper.

Different methods have been developed to prepare Pt-based electrocatalysts with cerium oxide, such as solid-state reactions under microwave irradiation [8], electrochemical processes [26], wet precipitation and reduction [27], sodium borohydride reduction [28], and co-precipitation [29]. In the work reported here, Pt-Ce based electrocatalysts were prepared by the polymeric precursor method (PPM) [30,31]. In the PPM, metallic salts are dissolved in a mixture of ethylene glycol (EG) and citric acid (CA), producing a polyester network containing metallic ions dispersed homogeneously. The polymeric solutions are applied to the support, and the final product, generally a metal oxide, is obtained by calcination at appropriate temperatures. This method has several advantages when compared to similar methods. The experimental procedure is extremely simple and the metallic precursors used are not sensitive to water, as is the case with the traditional sol–gel method, where metal alkoxides are used as precursors. Other advantages include the easy control of several variables that can lead to different defect densities or even to phase segregation in the final product, the direct decomposition of $(NH_3)_4PtCl_2$, the salt solubility at room temperature, and the low decomposition temperature. It is important to stress that the PPM method was already successfully used to prepare nanostructured materials with enhanced performance for methanol and ethanol oxidations [16,19,30,32].

The electrocatalysts produced were characterized by X-ray diffraction (XRD), transmission electron microscopy (TEM), energy dispersive analysis of X-rays (EDAX), and cyclic voltammetric (CV) measurements. The electrocatalytic activity was evaluated by CV and chronoamperometry (CA). The aim of this work is to use PPM for the preparation of Pt-CeO_2/C electrocatalysts (to our best knowledge this is the first time this method is used for this purpose) with different mass ratios between Pt and CeO_2, and to determine the best catalyst composition for the ethanol oxidation reaction in acidic solutions. For all compositions studied, 20 wt.% of active material (Pt-CeO_2) on carbon was used.

2. Experimental

2.1. Preparation of Pt-CeO_2/C electrocatalysts

The electrocatalysts were prepared using different mass ratios of Pt:CeO_2 (1:0, 3:1, 2:1, 1:1, 1:2, 1:3, and 0:1, with the maximum Pt loading of 0.15 mg cm^{-2}) using the polymeric precursor method as described by Freitas et al. [19] and the mass proportion 1:50:300 (metallic precursor:CA:EG). After preparation, the polymeric resins were refrigerated. For catalyst preparation, a measured volume of each resin was placed in an appropriate amount of carbon vulcan XC-72R (from Cabot), followed by the addition of excess EG that is just enough to cover the carbon powder. These mixtures were homogenized in an ultrasonic bath for 60 min, then thermally treated at 400 °C for 2 h in an N_2 atmosphere.

2.2. Physical characterization

XRD patterns of the catalyst samples were recorded in a Rigaku diffractometer (Miniflex model) using Cu-Kα radiation (1.541 Å, 30 kV and 15 mA). Catalyst compositional information was acquired in a Noran System Six X-ray microanalysis system operating at 30 kV in a JEOL JSM-5900LV scanning electron microscope (SEM). Morphological information on the catalysts was obtained via TEM using a FEI Tecnai G2 20 microscope operating at 200 kV. The samples were prepared by ultrasonication of the catalyst powders in isopropanol. A drop of the resulting dispersion was placed on thin carbon films deposited on standard TEM copper grids and dried in air. The images were acquired after surveying many different areas of the samples, in order to assess its average characteristics.

2.3. Electrochemical measurements

Electrochemical measurements were performed at room temperature (T = 25 °C) using an Autolab PGSTAT 302N potentiostat. Glassy carbon electrodes were used (support for the working electrodes with 0.166 cm^2 of geometric area), as were a Pt counter electrode and a reversible hydrogen electrode as the reference. The GC support was polished to a mirror finish with 1 μm of alumina suspension, and washed in a water/ethanol mixture before each experiment. The water used in all experimental procedures was obtained from a Milli-Q system from Millipore®.

The working electrodes were constructed by dispersing 10 mg of electrocatalyst powder in 1 mL water and mixing for 5 min in an ultrasonic bath. After this procedure, 20 μL of Nafion® solution (5%) was added to the suspension, and it was mixed again in an ultrasonic bath for 15 min. 16 μL aliquots of the dispersion fluid were pipetted onto the glassy carbon support surface. Finally, the

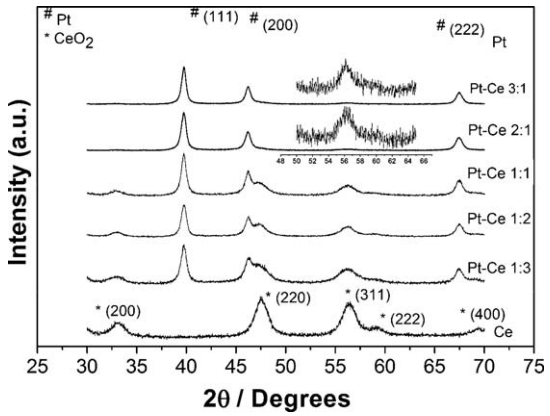

Fig. 1. X-ray diffraction patterns of Pt/C, PtCe/C, Ce/C electrocatalysts.

electrode was dried at 60 °C for 20 min, and finally hydrated for 5 min in water.

The cyclic voltammetric and chronoamperometric experiments were performed in 0.5 mol L^{-1} $HClO_4$ solution in the absence and in the presence of 0.5 mol L^{-1} of ethanol. The electrochemical cell was purged for 15 min with N_2 before each experiment.

3. Results and discussion

3.1. Characterization of Pt-CeO_2/C electrocatalysts

3.1.1. X-ray diffraction analysis

It has been reported in the literature that XRD data of crystalline compounds allows for estimation of the average particle size by the Debye–Scherrer formula, and that the value obtained deviates less than 6% compared with values obtained by TEM [33]. Thus, XRD analysis was performed to estimate the mean crystallite sizes and for structural characterization of the catalysts.

Fig. 1 shows the XRD patterns of the catalysts produced in several mass ratios. The patterns show characteristic diffraction peaks attributed to CeO_2 [34] (1 1 1), (2 0 0), and (3 1 1) planes centered at 28.5°, 46.6° and 55.7°, respectively, which are typical of single-phase oxides with fluorite structures. The broadening of the CeO_2 diffraction peaks is a characteristic of their small particle sizes. The face-centered cubic (FCC) structure of Pt is also apparent at $2\theta = 39.7°$ (1 1 1), $2\theta = 46.3°$ (2 0 0) and $2\theta = 67.45°$ (2 2 0) (JCPDS PDF#04-0802), which is similar to the XRD pattern of Pt/C composites [28,35,36]. Since the diffraction peaks associated with CeO_2 in the Pt-CeO_2/C 1:2 and 1:3 composites are highly attenuated in comparison with the Pt signal, they have been magnified to better visualize these results. Similar features observed in other CeO_2 containing catalysts are also clearly observed in these composites.

Table 1
XRD results for the Pt/C, PtCeO_2/C, CeO_2/C, and PtRu/C ETEK electrocatalysts.

Electrocatalyst	Mean Crystallite Size (nm)	
	Pt	CeO_2
Pt/C	7	–
PtCeO_2/C (3:1)	7	3
PtCeO_2/C (2:1)	7	3
PtCeO_2/C (1:1)	7	3
PtCeO_2/C (1:2)	5	3
PtCeO_2/C (1:3)	4	3
Ce/C	–	4
PtRu/C ETEK[a]	2–4	

[a] Data obtained from Ref. [43].

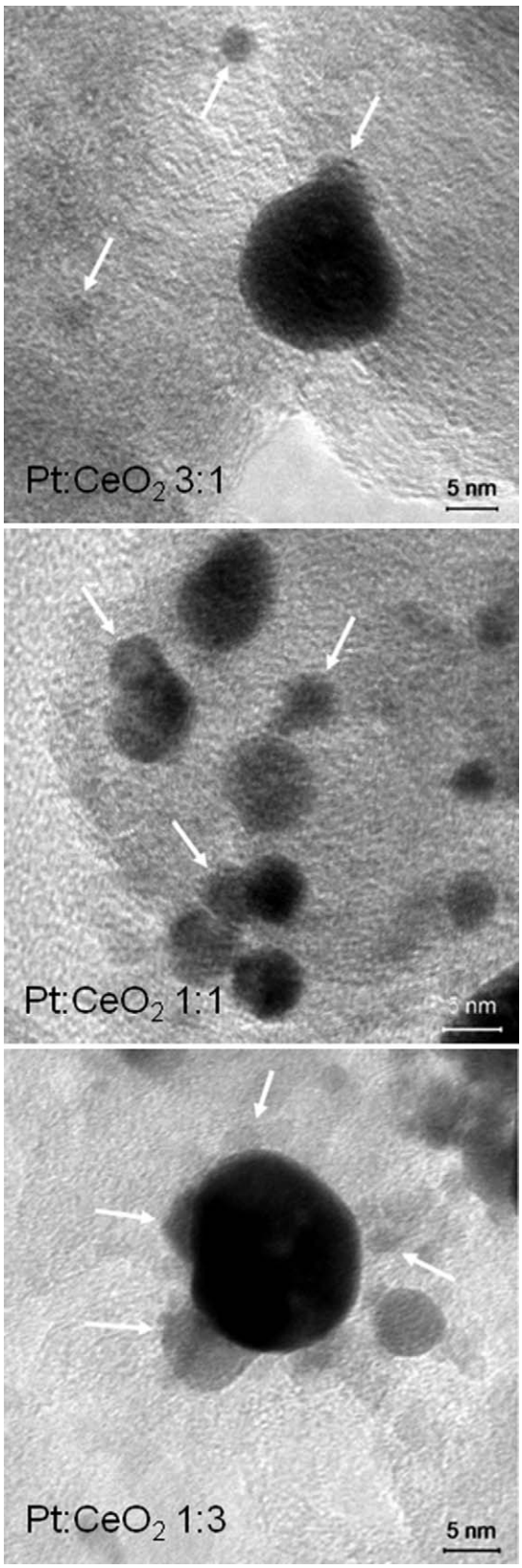

Fig. 2. Representative bright-field TEM images of PtCeO_2/C catalysts prepared with metal ratios of 3:1, 1:1, and 1:3.

The mean crystallite sizes of the Pt and CeO_2 particles were estimated using the Debye–Scherrer equation [37] and Winfit 1.2 software [38] at the crystalline planes ((1 1 1): $2\theta = 39.7°$) and ((3 1 1): $2\theta = 55.70$), respectively. The results are presented in

Table 1. The mean crystalline sizes of Pt were between 4 and 7 nm, whereas, for CeO_2, they were between 3 and 4 nm, in good agreement with the literature [22,28]. The results presented in Fig. 1 also show that the synthesized composites are composed of segregated nanocrystalline deposits without any indication of alloy phase formation between Pt and CeO_2. This is supported by the appearance of the diffraction peaks, relative to the Pt deposits, that are always at the same angle in all formulations studied.

At this point, it is important to stress that the PPM allows for the control of the particle size, mainly for Ce, which is close to 3 nm in all electrocatalysts containing Ce. Furthermore, for Pt, the particle sizes were always smaller than 7 nm, which is the best value for electrocatalysis applications [39]. The best catalytic performance was observed for the compositions where the Pt particles had small sizes, as discussed in Section 3.2.

3.1.2. Transmission electron microscopy

Fig. 2 shows TEM representative micrographs of the catalysts prepared with Pt:CeO_2 mass ratios of 3:1, 1:1, and 1:3, as indicated in the images.

Catalyst metal nanoparticles appear darker than the carbon support. For all Pt:CeO_2 catalysts, two distinguished particle sizes are seen, corroborating the results obtained by XRD: the smallest CeO_2 nanoparticles, indicated by white arrows, are positioned throughout the carbon support and nearby the biggest Pt nanoparticles. It is also observed that the fraction of small particles grows, in relation to the number of Pt particles, following the increase in the CeO_2 content. In fact, it has already been described in the literature that for $PtCeO_2$ systems, the particle size of catalyst systems measured from XRD is consistent with those obtained by TEM measurements [40]. Furthermore, the same work showed a decrease in Pt particle size in ceria-incorporated catalysts compared to ceria-free Pt catalysts, substantiated by TEM observations, as is observed here. In that work, a gradual decrease in pore diameter of the catalyst systems below 2.5 nm were also noted with increased ceria content. It appears that ceria deposits at the micropores of the carbon support, reducing the micropore volumes in the carbon.

3.1.3. Energy dispersive X-ray analysis

EDAX analyses were used to determine the composition of the materials prepared by the PPM. Table 2 summarizes the results obtained for the different compositions. Except for a small deviation from the theoretical value expected for the $PtCeO_2$/C (3:1) catalyst, there is a good agreement between the experimental data and the ratios used in the preparation of the composites, confirming the accuracy of the method.

Table 2
Composition of the Pt/C, PtCe/C, and Ce/C electrocatalysts obtained from EDAX measurements.

Catalyst	EDAX mass %	
	Pt	Ce
Pt/C	100	–
PtCe/C (3:1)	70	30
PtCe/C (2:1)	67	33
PtCe/C (1:1)	40	60
PtCe/C (1:2)	33	67
PtCe/C (1:3)	26	74
Ce/C	–	100

3.1.4. Electrochemical characterization

Fig. 3a shows the cyclic voltammetric profiles for Pt/C, PtRu/C ETEK, and Pt-CeO_2/C electrocatalysts in 0.5 mol L^{-1} $HClO_4$ solution. For the Pt/C electrode, the voltammetric profile presents a fair resolution of the platinum features as widely discussed elsewhere [41–43]. For the PtRu/C ETEK electrocatalyst, a single hydrogen desorption peak (dotted line) is observed in the potential range from 0.05 to 0.3 V, which is in agreement with previously reported results available in the literature [35,44]. The partial inhibition of the voltammetric peaks of the Pt/C catalyst, as well as the very high capacitive current observed in all cases, are typical responses of carbon dispersed metal catalysts when the experiment is conducted in aqueous electrolytes solutions.

For the Pt-CeO_2 electrocatalysts (Fig. 3b), broader hydrogen adsorption/desorption peaks are found in the potential range from 0.05 to 0.4 V. Good definition for the H UPD desorption and adsorption peaks is found, where the current intensity associated with these processes is directly proportional to the increased platinum proportion in the composites. This effect can be related to a higher number of active sites available for H adsorption/desorption, which results from the enrichment of Pt atoms in the catalysts surfaces containing high platinum ratios. For the electrodes with higher CeO_2 and lower Pt contents, smaller hydrogen desorption/adsorption peaks and double-layer charging current are observed, which is in accordance with data obtained in the literature [35].

If the structural features of the Pt-CeO_2/C catalysts shown by the XRD measurements, and the absence of faradaic processes in the potential range from 0.05 to 0.4 V in the cyclic voltammetric profile of CeO_2/C composite (Fig. 3a) are taken into account, it is reasonable to assume that the voltammetric peaks associated with the H adsorption/desorption processes occurring on the Pt surface in the CeO_2 catalysts are not affected by the presence of ceria. Thus,

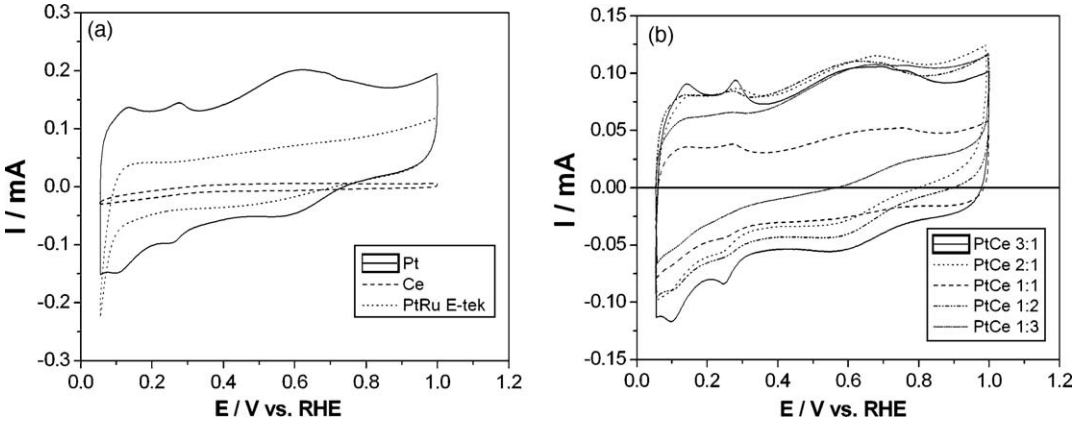

Fig. 3. Cyclic voltammograms of (a) Pt/C, Ce/C and (b) PtCe/C in ratios 3:1, 2:1, 1:1, 1:2, and 1:3 in 0.5 mol L^{-1} $HClO_4$ aqueous solution at room temperature at a potential sweep rate of 10 mV s^{-1}. T = 25 °C.

Table 3
Catalytic activities for ethanol electro-oxidation showing the onset potential and mass activity toward that reaction in the different electrocatalysts studied.

Catalyst	Onset Potential (V *vs.* RHE)	I_m (mA mg^{-1} Pt)	Specific surface area of Pt m^2 g^{-1}
Pt/C	0.34	131	8.38
PtCe/C (3:1)	0.23	115	7.53
PtCe/C (2:1)	0.25	10S	7.12
PtCe/C (1:1)	0.28	104	5.24
PtCe/C (1:2)	0.29	191	15.13
PtCe/C (1:3)	0.30	225	15.38
PtRu/C ETEK	0.25	95	–

the charges associated with the H desorption process from 0.05 to 0.4 V can be used to calculate the electroactive surface areas for all Pt-CeO_2/C catalysts. The mass of Pt in all formulations (using the Pt wt.% from the EDAX results) can be used to determine the specific surface area of Pt (defined as the ratio between electroactive area and the mass of Pt in each catalyst), and is summarized in Table 3. From these results, it can be observed that catalysts with lower Pt contents have higher specific surface areas ($PtCeO_2$/C 1:3 and $PtCeO_2$/C 1:2). Otherwise, the specific surface area of catalysts with higher Pt contents diminishes as the Pt amount decreases from $PtCeO_2$/C 3:1 up till $PtCeO_2$/C 1:1. These results are in good agreement with those provided by the XRD measurements, which show that catalysts with lower Pt contents also have the lowest mean crystallite size.

3.2. Electrocatalytical activity of the materials toward ethanol oxidation

For reasons explained above, the electrocatalytic activity results of the Pt-CeO_2/C electrodes toward ethanol oxidation will be compared with those obtained for a commercially available PtRu/C Etek, as well as with Pt/C.

Fig. 4 shows the cyclic voltammetric curves of ethanol electro-oxidation on Pt/C, PtRu/C ETEK, and Pt-CeO_2/C (1:3) electrocatalysts. The potentials were scanned from 0.05 to 1 V at a scan rate of 5 mV s^{-1}. Oxidation currents were observed during both forward and backward scans. In this work, mass current densities (or mass activity, I_m, defined as the ratio between the current and the mass of Pt [45]), were used instead of current in the voltammetric experiments in Fig. 4 to evaluate the catalytic activity of the different compositions. The results for the peak current in the forward scan together with the onset potentials obtained for the different catalysts studied are presented in Table 3.

Table 3 clearly shows that the modification of Pt with CeO_2 results in composites with superior catalytic activities for the ethanol oxidation reaction. The onset potential for this reaction is highly affected by the incorporation of ceria, and is dependent on the Pt-to-ceria ratio. The lowest onset potential was obtained for the catalyst with the highest Pt content (Pt-CeO_2/C 3:1, onset potential = 0.23 V), which is lower than that obtained for Pt/C (0.34 V), and very close to the value obtained for the PtRu ETEK (0.25 V) catalyst. This is an expected result since the capacity to absorb organic molecules at low potentials is higher in composites with high platinum contents. In contrast, the highest mass activity was obtained for catalysts containing smaller amounts of Pt (Pt-CeO_2 (1:3)), for which the maximum value of 225 mA mg^{-1} Pt at around 0.9 V in the forward scan was recorded. At this potential, the mass activity of Pt-CeO_2/C (1:3) is 1.95 times the mass activity of the Pt-CeO_2/C (3:1) catalyst. To better explain this behavior, the specific surface area of the different ceria modified catalysts must be considered. Although mass activity is one way to evaluate the activity of electro-catalysts, it is a function of the specific surface area of Pt [29]. Indeed, it has been demonstrated that mass activity increases with an increase in specific surface area of Pt (m^2/g) [46,47].

Using an activity scale based on the mass activity presented in Table 3 to compare the performance of the different Pt-CeO_2/C catalysts, the order followed is rigorously the same as that found for the specific surface area of Pt (Table 3): PtCe (1:3) > PtCe (1:2) > PtCe (3:1) > PtCe (2:1) > PtCe (1:1). This is a very interesting result, which shows that for Pt-CeO_2 catalysts, the specific surface area of Pt is maximized in composites with higher CeO_2 contents. It is especially interesting from as economic perspective, since ceria is much cheaper than Ru, and, as will be demonstrated later in this paper, the catalytic performance of Pt-CeO_2/C with lower Pt to CeO_2 mass ratios is higher than the performance of PtRu/C for the electro-oxidation of ethanol.

Other different effects may also contribute to the higher mass activity observed on the considered catalysts: i) The poisoning by

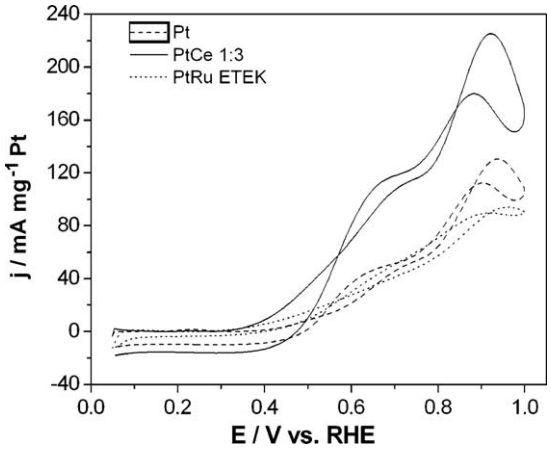

Fig. 4. Cyclic voltammograms of Pt/C, PtCe/C 1:3 and the commercial PtRu/C (ETEK) in 1.0 mol L^{-1} CH_3CH_2OH + 0.5 mol L^{-1} $HClO_4$ aqueous solution at room temperature at a potential sweep rate of 10 mV s^{-1}. T = 25 °C.

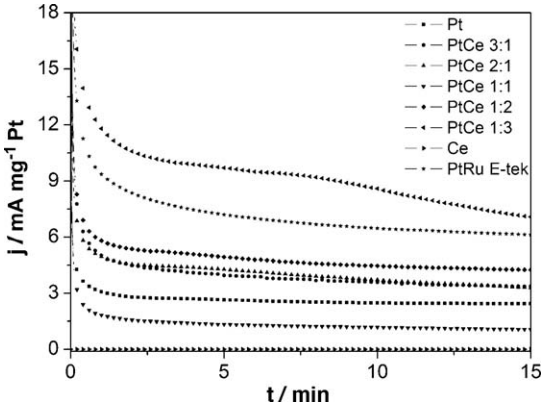

Fig. 5. Chronoamperometry curves for the 20 wt.% of all electrocatalysts on carbon in 1.0 mol L^{-1} CH_3CH_2OH + 0.5 mol L^{-1} $HClO_4$. $E_{oxidation}$ = 0.5 V, time = 15 min. T = 25 °C.

strongly bounded intermediates, such as CO_{ads}, is lower in these cases, resulting in a much more effective participation of CeO_2 in supplying OH_{ads} to eliminate the poisoning intermediates. It should be mentioned that Pt-CeO_2 is a proven efficient catalyst for low temperature water–gas-shift reaction when the Pt loading is low [25]. ii) Although activating the C–C bond of ethanol on Pt is difficult, a synergistic effect produced by the combination of Pt with CeO_2 can facilitate this process, allowing the complete oxidation of ethanol to CO_2. This must first be proven, and will be the focus of our future efforts. iii) Pt-CeO_2/C (1:3) was the composite where the Pt particle size exhibited the lowest value (4 nm) as indicated in Table 2. It has already been demonstrated that the particle size is a key parameter in the catalytic process, especially in the case of Pt based materials [48]. It has been established that in catalysts with a face-centered cubic unit cell conformation, particles larger than 4 nm do not contribute significantly to a higher catalytic activity.

In order to confirm the results obtained in the cyclic voltammetric experiments, chronoamperometric measurements were performed in 0.5 mol L^{-1} $HClO_4$ + 1 mol L^{-1} CH_3CH_2OH solutions by applying a potential step from 0.05 to 0.5 V, and then evaluating the responses of current-time after 15 min of polarization. Fig. 5 depicts the results obtained for several compositions of Pt-CeO_2/C, for Pt/C, and PtRu ETEK (the last two for comparative purposes). The potential of 0.5 V was chosen because above this potential there is no practical importance to fuel cell applications. In all cases, a sharp initial current drop in the first 5 min, followed by a slow decay is observed. The current density on the Pt/C electrode decreases to values near 2.4 mA mg^{-1} Pt after 15 min of polarization, which is higher only than the values obtained for CeO_2/C and Pt-CeO_2 (1:1). Other important information obtained from the results depicted in Fig. 4 is that, except for the catalyst Pt-CeO_2/C (1:1), the current decreases with increasing Pt content after 15 min of polarization. The best performance was obtained for the Pt-CeO_2/C (1:3) electrocatalyst (current density = 7 mA mg^{-1}Pt after 15 min of polarization *vs.* 6.1 mA mg^{-1}Pt for PtRu/C ETEK).

The experimental data obtained in the chronoamperometric experiments was used to verify the influence of the catalyst composition in the catalysis of ethanol electro-oxidation. Thus, the current measured after 15 min polarization at 0.5 V was plotted *vs.* the percentage of Ce in the different compositions evaluated, as presented in Fig. 6. Such a comparison has been used in similar work for Pt-Ru catalysts [49]. When compared with the results reported in literature [48] (mainly the shape of the curve), some fundamental differences can be seen.

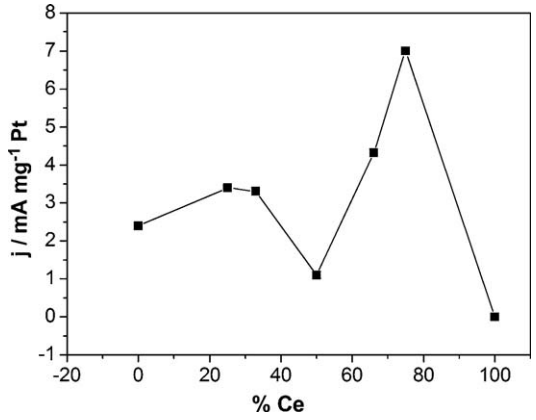

Fig. 6. Activity toward ethanol electro-oxidation as a function of PtCe composition. The data were obtained from chronoamperometric curves after 15 min of electrocatalysts polarization at 0.5 V in 1.0 mol L^{-1} CH_3CH_2OH + 0.5 mol L^{-1} $HClO_4$. T = 25 °C.

For Pt-Ru catalysts, the curve exhibits a steep increase above 20% Ruthenium composition, and although the establishment of the exact position of the maximum could not be determined, the shape of the curve was explained as follows: adsorption and dissociation of ethanol occurs only to a limited extent [50], and takes place mainly on Pt sites. Oxidation of adsorbed residues [45,51] requires H_2O dissociation (or activation [52]), and at the potential of 0.5 V, this process occurs mainly on Ru. Thus, a bi-functional [48,53] mechanism seems to be operative. At low Ru concentrations, there are not enough Ru sites to effectively assist the oxidation of adsorbed residues, and the oxidation current remains close to the levels obtained for pure Pt. On ceria-based catalysts, a small enhancement in the current density for ethanol oxidation is observed for catalysts containing up to 25% of Ce when compared to Pt/C. This enhancement can be attributed to the release of oxygen atoms by the CeO_2 particles [28] that can easily react with some atoms of Pt on the surface (as suggested for Ru in the methanol oxidation reaction), because of their higher oxophilic character, forming PtO_x species as indicated in the following reactions:

$$CeO_2 \rightarrow CeO_{2-x} + \tfrac{x}{2}O_2 \quad (1)$$

$$Pt + \tfrac{x}{2}O_2 \rightarrow PtO_x \quad (2)$$

This explains the lowering of the onset potential for ethanol oxidation compared to Pt (at 25% of Ce on Pt) as shown in Table 3. For a Ce content higher than 25%, the current densities decrease steeply. This behavior is completely different from that observed for Pt-Ru catalysts, where the current densities on catalysts with a Ru content higher than 25% increase steeply, and a Pt:Ru ratio of 60:40 seems to present a site distribution close to the optimum for ethanol oxidation. For ceria-based materials, the electrocatalytic performance follows the same activity scale as previously observed in the cyclic voltammetric experiments. Thus, for a Ce content up to 50%, the decrease of the current densities for ethanol oxidation is due to a lowering in the specific surface area of Pt in the different catalysts considered. This also explains the lowest mass activity achieved for the catalyst containing the Ce to Pt mass ratio of (1:1). Using the results obtained in the chronoamperometric experiments, a more complete activity scale can be constructed in which the Pt/C and PtRu/C catalysts are now included: PtCe (1:3) > PtRu > PtCe (1:2) > PtCe (3:1) > PtCe (2:1) > Pt > PtCe (1:1). It is clear from this activity scale that ceria can effectively enhance the catalytic performance of Pt based materials toward the ethanol oxidation reaction, but only if the specific surface area of Pt is not seriously affected by the addition of Ce. At this point, it is important to emphasize that the common behavior of a bi-

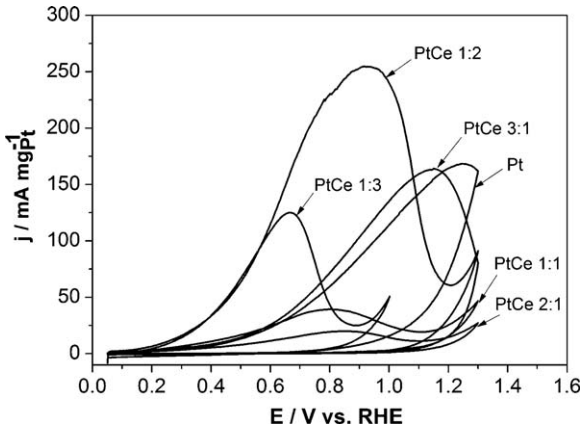

Fig. 7. CO-stripping curves using Pt and ceria-incorporated Pt-supported catalysts.

functional mechanism was not observed in Pt-CeO_2/C materials used here for ethanol oxidation.

Since CO is one of the main poisoning intermediates produced by the electro-oxidation of ethanol at the surface of platinum-based electrocatalysts, it is advantageous that $PtCeO_2$ catalysts may assist in the oxidative removal of this poisoning intermediate at potential values lower than is observed for unmodified Pt catalysts. This ability can be verified by using CO-stripping tests as already described for the methanol oxidation reaction using the same catalysts [40]. This information may provide insight on the mechanism behind the enhanced activity of Pt-CeO_2/C catalysts for ethanol electro-oxidation. As observed in Fig. 7, for ceria-incorporated platinum catalysts, the onset potential is shifted to lower values compared to unmodified Pt materials. This feature has already been observed when the same material was used for the methanol oxidation [40]. Fig. 7 indicates that lowest onset potential toward CO oxidation was obtained for the PtCe 1:3 electrocatalyst.

In this case, the onset potential for CO oxidation is 0.15 V, almost identical to that observed for the PtCe 1:2 electrocatalyst. The peak currents for the oxidation of CO are centered at the potentials of 0.65 V for PtCe 1:3, and at 0.95 V for PtCe 1:2. The higher peak current observed for the CO oxidation on the PtCe catalyst 1:2 may be due to a higher amount of CO adsorbed on the surface of this material. Consequently, the covering of the PtCe 1:3 catalyst surface is lower in the later case. As the specific surface of Pt is similar in both catalysts and the current is normalized by the mass of Pt, it is very reasonable to assume that the affinity of CO for the active sites in PtCe 1:3 is lower, and that the consequent covering of the surface by this product is lower, resulting in reduced peak currents as observed in Fig. 7. Thus, the best average catalytic performance for the ethanol oxidation observed for the Pt-CeO_2/C (1:3) catalyst may also be a result of a higher CO tolerance. The results obtained in the present work showed that Pt-CeO_2/C catalysts prepared by the PPM method are promising candidates to be used at the anodes of direct ethanol fuel cells. To elucidate the mechanism of ethanol oxidation on Pt-CeO_2/C catalysts, further work must be performed.

4. Conclusions

Pt-CeO_2/C powders were prepared, characterized, and tested as electrocatalysts for ethanol oxidation in an acidic medium. The XRD results indicate that the materials prepared by the PPM method produced mean crystallite sizes between 3 and 7 nm for Pt, between 3 and 4 nm for CeO_2. This catalyst particle size distribution was confirmed by TEM imaging. The mass ratios among Pt and CeO_2 oxides were confirmed using EDAX. The results of cyclic voltammetry and chronoamperometry showed that Pt-CeO_2/C (1:3) has a higher ethanol electro-oxidation activity compared to both Pt/C and PtRu/C ETEK materials. The higher catalytic activity was attributed to several intrinsic features, such as reduced poisoning by the strongly bounded intermediates, and maximum utilization of the catalyst surface for particle sizes $\leq$4 nm. From an economical perspective, and considering the results obtained, Pt-CeO_2/C electrocatalysts prepared by the PPM method are promising candidates for use as catalysts in anodes of direct ethanol fuel cells.

Acknowledgements

The authors wish to thank the Brazilian Funding Institutions CNPq, CAPES, and FAPESP (Process Number: 05/59992-6), and UFABC for their financial support. In addition, the authors thank Prof. Vera R.L. Constantino from IQ-USP for the use of XRD instrument, and Dr. Ângela A. Teixeira Neto for assistance with XRD analysis. ETN thanks LME-LNLS for the use of the JEOL JSM-5900LV microscope and LAMM-CETENE for the TEM images acquisition.

References

[1] S. Rousseau, C. Coutanceau, C. Lamy, J.-M. Leger, J. Power Sources 158 (2006) 18–24.
[2] C.Y. Chen, P. Yang, J. Power Sources 123 (2003) 37–42.
[3] F. Vigier, C. Coutanceau, A. Perrard, E.M. Belgsir, C. Lamy, J. Appl. Electrochem. 34 (2004) 439–446.
[4] C. Lamy, S. Rousseau, E.M. Belgsir, C. Coutanceau, J.-M. Léger, Electrochim. Acta 49 (2004) 3901–3908.
[5] E.V. Spinacé, A.O. Neto, M. Linardi, J. Power Sources 129 (2004) 121–126.
[6] L.H. Jiang, Z.H. Zhou, W.Z. Li, W.J. Zhou, S.Q. Song, H.Q. Li, G.Q. Sun, Q. Xin, Energy Fuels 18 (2004) 866–871.
[7] H. Wang, Z. Jusys, R.J. Behm, J. Phys. Chem. B 108 (2004) 19413–19424.
[8] C. Xu, P.K. Shen, J. Power Sources 142 (2005) 27–29.
[9] X. Ren, T.E. Springer, T.A. Zawodzmski, S. Gottesfeld, J. Electrochem. Soc. 147 (2000) 466–474.
[10] K. Scott, W.M. Taama, P. Argyropoulos, K. Sundmacher, J. Power Sources 83 (1999) 204–216.
[11] V. Pacheco Santos, G. Tremiliosi-Filho, J. Electroanal. Chem. 554–555 (2003) 395–405.
[12] E. Antolini, J. Power Sources 170 (2007) 1–12.
[13] A. Ghumman, C. Vink, O. Yepez, P.G. Pickup, J. Power Sources 177 (2008) 71–76.
[14] V. Rao, C. Cremers, U. Stimming, L. Cao, S. Sun, S. Yan, G. Sun, Q. Xin, J. Electrochem. Soc. 154 (2007) B1138–B1147.
[15] H. Li, G. Suna, L. Cao, L. Jiang, Q. Xin, Electrochim. Acta 52 (2007) 6622–6629.
[16] F.C. Simões, D.M. dos Anjos, F. Vigier, J.-M. Léger, F. Hahn, C. Coutanceau, E.R. Gonzalez, G. Tremiliosi-Filho, A.R. de Andrade, P. Olivi, K.B. Kokoh, J. Power Sources 167 (2007) 1–10.
[17] A.O. Neto, R.R. Dias, M.M. Tusi, M. Linardi, E.V. Spinace, J. Power Sources 166 (2007) 87–91.
[18] H.M. Villullas, F.I. Mattos-Costa, L.O.S. Bulhoes, J. Phys. Chem. B 108 (2004) 12898–12903.
[19] R.G. Freitas, L.F. Marchesi, R.T.S. Oliveira, F.I. Mattos-Costa, E.C. Pereira, L.O.S. Bulhões, M.C. Santos, J. Power Sources 171 (2007) 373–380.
[20] G.R. Salazar-Banda, H.B. Suffredini, M.L. Calegaro, S.T. Tanimoto, L.A. Avaca, J. Power Sources 162 (2006) 9–20.
[21] J. Shim, C. Lee, H. Lee, J. Lee, E.J. Cairns, J. Power Sources 102 (2001) 172–177.
[22] Y. Bai, J. Wu, J. Xi, J. Wang, W. Zhu, L. Chen, X. Qiu, Electrochem. Commun. 7 (2005) 1087–1090.
[23] C. Xu, P.K. Shen, X. Ji, R. Zeng, Y. Liu, Electrochem. Commun. 7 (2005) 1305–1308.
[24] C. Xu, P.K. Shen, Chem. Commun. 19 (2004) 2238–2241.
[25] Q. Fu, H. Saltsburg, M. Flytzani-Stephanopoulos, Science 301 (2003) 935–938.
[26] C.L. Campos, C. Roldan, M. Aponte, Y. Ishikawa, C.R. Cabrera, J. Electroanal. Chem. 581 (2005) 206–215.
[27] Z. Tang, G. Lu, J. Power Sources 162 (2006) 1067–1072.
[28] J.W. Guo, T.S. Zhao, J. Prabhuram, R. Chen, C.W. Wong, J. Power Sources 156 (2006) 345–354.
[29] Y. Bai, J. Wu, X. Qiu, J. Xi, J. Wang, J. Li, W. Zhu, L. Chen, Appl. Catal. B: Environ. 73 (2007) 144–149.
[30] R.G. Freitas, M.C. Santos, R.T.S. Oliveira, L.O.S. Bulhões, E.C. Pereira, J. Power Sources 158 (2006) 164–168.
[31] R.G. Freitas, R.T.S. Oliveira, M.C. Santos, L.O.S. Bulhões, E.C. Pereira, Mater. Lett. 60 (2006) 1906–1910.
[32] L.P.R. Profeti, F.C. Simões, P. Olivi, K.B. Kokoh, C. Coutanceau, J.-M. Leger, C. Lamy, J. Power Sources 158 (2006) 1195–1201.
[33] K.J.J. Mayrhofer, J.C. Meier, S.J. Ashton, G.K.H. Wiberg, F. Kraus, M. Hanzlik, M. Arenz, Electrochem. Commun. 10 (2008) 1144–1147.
[34] X-ray Powder Diffraction Standards, ASTM, Philadelphia, PA, Card 34-394 (CeO_2).
[35] J.W. Guo, T.S. Zao, J. Prabhuram, C.W. Wong, Electrochim. Acta 50 (2005) 1973–1983.
[36] H.B. Yu, J.-H. Kim, H.-I. Lee, M.A. Schibioh, J. Lee, J. Han, S.P. Yoon, H.Y. Ha, J. Power Sources 140 (2005) 59–65.
[37] B.D. Cullity, Elements of X-ray Diffaction, 3rd ed., Addison-Wesley, Massachusetts, 1967, p. 262.
[38] H.B. Suffredini, V. Tricoli, N. Vatistas, L.A. Avaca, J. Power Sources 158 (2006) 124–128.
[39] K.J.J. Mayrhofer, B.B. Blizanac, M. Arenz, V.R. Stamenkovic, P.N. Ross, N.M. Markovic, J. Phys. Chem. B 109 (2005) 14433–14440.
[40] M.A. Scibioh, S. Kim, E.A. Cho, T.H. Lim, S.A. Hong, H.Y. Ha, Appl. Catal. B Environ. 84 (2008) 773–782.
[41] J.G. Oh, C.H. Lee, H. Kim, Electrochem. Commun. 9 (2007) 2629–2632.
[42] Z. Liu, B. Guo, L. Hong, T.H. Lin, Electrochem. Commun. 8 (2006) 83–90.
[43] E.V. Spinacé, A.O. Neto, T.R.R. Vasconcelos, M. Linardi, J. Power Sources 137 (2004) 17–23.
[44] W.H. Lizcano-Valbuena, V.A. Paganin, E.R. Gonzalez, Electrochim. Acta 47 (2002) 3715–3722.
[45] V. Raghuveer, A. Manthiram, J. Electrochem. Soc. 152 (2005) A1504–A1510.
[46] M. Watanabe, S. Saegusa, J. Electroanal. Chem. 271 (1989) 213–220.
[47] J.H. Zeng, J.Y. Lee, W.J. Zhou, Appl. Catal. A: Gen. 208 (2006) 99–104.
[48] F. Raimondi, G.G. Scherer, R. Kötz, A. Wokaun, Angew. Chem. Int. Ed. 44 (2005) 2190–2209.

[49] G.A. Camara, R.B. de Lima, T. Iwasita, Electrochem. Commun. 6 (2004) 812–815.
[50] T. Iwasita, E. Pastor, Electrochim. Acta 39 (1994) 531–537.
[51] Z. Liu, X.Y. Ling, X. Su, J.Y. Lee, L.M. Gan, J. Power Sources 149 (2005) 1–7.
[52] H. Kim, I. Rabelo de Moraes, G. Tremiliosi-Filho, R. Haasch, A. Wieckowski, Surf. Sci. 474 (2001) L203–L212.
[53] W.J. Zhou, W.Z. Li, S.Q. Song, Z.H. Zhou, L.H. Jiang, G.Q. Sun, Q. Xin, K. Poulianitis, S. Kontou, P. Tsiakaras, J. Power Sources 131 (2004) 217–223.